Electroconductive Tantalum-Based Coatings for Bioelectronic Bone Implants: Fabrication, Characterisation, and Neural Interface Applications

J. K. Annan[1]*, L. Gyansah[2]

[1]University of Mines and Technology, Tarkwa, Ghana

[2]Assemblies of God, Institute of Higher Learning, Krunum-Afrancho, Ghana

***Corresponding Author**

DOI: https://doi.org/10.51584/IJRIAS.2025.10120008

Received: 13 December 2025; Accepted: 21 December 2025; Published: 01 January 2026

ABSTRACT

To improve the bioelectrical conductivity, bioactivity, and biocompatibility of titanium implants, an electroconductive tantalum (Ta) coating was fabricated on Ti6Al4V (TC4) substrates via the cold spray technique. Microstructural and phase characterizations were performed using Scanning Electron Microscopy (SEM), X-ray Diffraction (XRD), and Fourier-Transform Infrared Spectroscopy (FTIR). Four-point probe resistivity, Electrochemical Impedance Spectroscopy (EIS), and Cyclic Voltammetry (CV) were used to characterize electrical and electrochemical properties relevant to neural interfaces. Mechanical and bioactivity evaluations included tensile adhesion, three-point bending, and Vickers microhardness tests, alongside simulated body fluid (SBF) immersion to assess osteointegration potential. Results show that the cold-sprayed Ta coating exhibits a bulk electrical conductivity of 6.8×10^6 S/m, approximately 40 % that of pure bulk Ta, due to the presence of inter-particle interfaces and porosity. The coating's impedance at 1 kHz-a frequency range relevant to neural signal transmission was measured at ~8.2 kΩ·cm², indicating favorable charge transfer capability for neural electrode applications. The double-layer capacitance extracted from the EIS Nyquist plots was approximately 2.6 mF/cm², signifying strong electrochemical surface activity. Mechanically, the coatings exhibited an adhesive strength of 10.6 MPa, microhardness of 300 $HV_{0.1}$, and Young's modulus of 11.08 GPa, closely matching the modulus of natural cortical bone (10-30 GPa). Bioactivity assessment showed dense apatite layer formation within 14 days of immersion, while electrical stimulation (±100 µA, 1 Hz) significantly enhanced apatite nucleation rates, confirming electro-assisted biomineralization. These findings show improvement in bone-implant integration with emphasis on electrical performance suitable for bioelectronic and neural stimulation implants.

Keywords: Cold spray, Electroconductive coatings, Tantalum, Neural interface, Bioelectronics, Osteointegration, Impedance

INTRODUCTION

Overview of Bioelectronic Implants

The emergence of bioelectronic implants has expanded the functional requirements of orthopedic materials. Beyond mechanical and biological compatibility, modern implants must enable electrical interfacing with biological tissues for purposes such as electrostimulation-assisted healing, neural recording, and smart feedback sensing (Loi *et al.,* 2016; Oryan *et al*., 2014; Meyers *et al*., 2013; Simchi *et al*., 2011). These applications demand materials with moderate conductivity (10^4–10^6 S/m), low interfacial impedance, and chemical inertness in ionic environments.

While titanium and its alloys (e.g., Ti6Al4V) remain the mainstay of orthopedic implants, their intrinsically low conductivity (~2.4×10^6 S/m) limits their application in bioelectronic systems. Tantalum (Ta), by contrast, possesses superior electrical conductivity (~7.4×10^6 S/m), high corrosion resistance, and excellent

biocompatibility due to its stable Ta_2O_5surface film (bandgap ≈ 4.4 eV) that supports ionic exchange without significant Faradaic degradation (Chen *et al*., 2012; Chen and Thouas, 2015; Shabalin, 2014).

In addition, Ta exhibits dielectric polarization properties that make it favorable for capacitive charge transfer, a critical mechanism in neural interface electrodes where current density and charge injection capacity (CIC) determine neural stimulation safety. Typical CIC for Ta-based coatings is reported in the range 1–5 mC/cm², comparable to noble-metal electrodes such as platinum-iridium (Pt–Ir) (Lei *et al*., 2022; Alontseva *et al*., 2023).

Thus, a cold-sprayed Ta coating combines mechanical robustness, electrical conductivity, and electrochemical stability, positioning it as an ideal candidate for electroactive bone–neural implants capable of transmitting bioelectrical signals or delivering therapeutic currents.

Recent Happenings for Orthopedic Solutions

With more and more orthopedic diseases (Loi *et al*., 2016; Oryan *et al.*, 2014), people are trying to find effective ways to repair human bone. Different types of biomaterials have been used as materials for bone repairs (Meyers *et al*., 2013; Simchi *et al*., 2011; Chen *et al.*, 2012). Metallic biomaterials (Chen and Thouas, 2015) have been used more recently in surgery. Medical stainless steel, cobalt and titanium alloys, for example, are widely used in clinical practice. But titanium's biological properties are far from being what humans require and a fibrous layer may form at the skeletal tissue/device interface causing aseptic loosening of the device, which desires a lot of new material. Materials are turned from inert materials to bioactive materials. Therefore, whatever solution that can extend the life of prostheses will be welcomed by the clinical community.

Recently tantalum is gaining more attention as a new metallic biomaterial. Tantalum (Shabalin, 2014) is a heavy refractory metal with high melting point (approximately 3000 °C) and high density (16.65 g/cm^3). It has excellent chemical properties, extremely high corrosion resistance, owing to the stable tantalum pentaoxide (Ta_2O_5) protective film. There is a very small thermal expansion coefficient, moderate hardness and malleability of tantalum. Hence, it can be drawn into filaments and made into thin foil.

Adaptability of Tantalum

In medicine, tantalum is an ideal biomaterial (Lei *et al*., 2022; Alontseva *et al*., 2023; Balla *et al*., 2010a). It can be adapted to biological cells with excellent affinity, hardly stimulating and side effects in direct contact with human bone, muscle tissue and liquid. Argyropoulou *et al*. (2024), found spherical bone-like apatite on the surface of tantalum through the traditional biological performance test. Liu *et al*. (2025) studied the biocompatibility of tantalum through animal experiments. They implanted tantalum in the soft tissues and the femoral shaft of rats, and didn't find obvious inflammatory response and corrosion phenomenon around tantalum. These results proved that tantalum has good bioactivity and biocompatibility.

Tantalum Coatings

At present most studies of tantalum coatings are prepared by chemical vapor deposition (CVD) on porous carbon skeleton, or powder sintering process (Wei *et al*., 2015; Xinting *et al*., 2017). There are also some other preparations, such as plasma spraying, sputter deposition and laser engineered net shaping (LENS™) (Balla *et al.*, 2010b). However, there are still some drawbacks, such as high cost and high temperature where oxidation causes loss of ductility of metals. Thus, they need high vacuum or high purity protective atmosphere in order to avoid oxidation due to the high temperature in the process of spraying.

Compared with other metals, the content of tantalum is relatively low, which mainly exists in tantalite and co-exists with niobium (Melcher *et al*., 2017). But in view of the huge demand for tantalum in aerospace, electronics, medical and other industries, the deep processing of tantalum is an important task of tantalum industry. Since tantalum applications in biomedical devices have been limited by processing challenges rather than biological performance, it is of great significance to improve the processing capacity of tantalum. Due to the melting point of tantalum is nearly 3000 °C, the fabrication of tantalum has its particularity. Therefore, tantalum is extremely suitable for cold spraying (Schmidt *et al.*, 2006; Gartner *et al*., 2006). And that cold spraying as an emerging technology has been reported for biocompatible and antibacterial coatings (Vilardell *et al*., 2015).

ISSN No. 2454-6194 | DOI: 10.51584/IJRIAS |Volume X Issue XII December 2025

Cold Spraying

Cold spraying (Papyrin *et al*., 2006), also called kinetic spraying, is a kind of new technique with the temperature far lower than the melting point of the material. The particles reach a very high velocity through the gas acceleration, and hit the matrix, resulting in plastic deformation, which is combined with the substrate. Therefore, for metals with relatively high melting point, such as tantalum in this paper, cold spraying is a very effective means (Koivuluoto *et al*., 2010; Delloro *et al*., 2017; Kumar *et al*., 2016).Compared with other spraying coatings, the composition and microstructure of cold spraying coatings are consistent with the raw material powders, avoiding the performance degradation due to the high temperature which can result in phase transition. Hence, cold spraying is especially suitable for the preparation of sensitive materials (Moridi *et al*., 2014). This research will employ cold spraying technology to address electroconductive and thermal conductive coatings useful for bioelectronic bone implants. The paper addresses the fabrication of novel tantalum coatings, its microstructure characterization, and properties for neural interface applications.

Resources and Methods Used

In this study, a bioactive tantalum coating was fabricated by cold spraying technology to have a dense coatings. The kinetics of cold spraying process demonstrated that tantalum coatings can be produced with compressed air and have found not to react with the atmosphere (Neu *et al*., 2023). This cold spraying approach has the potential to deliver a more bioactive coating for advanced biomedical prostheses and implants. The powder used in this experiment was commercially available gas-atomized tantalum powder with a particle size d_{10} = 13.39 μm, mean= d_{50} = 26.24 μm and d_{90} = 41.71 μm probed by a laser particle size analyzer (see Fig.1. (b)). The surface morphology of Ta particles was observed using a Scanning Electron Microscopy (SEM) (Fig. 1(a)) and the morphology was irregular shape with some few particle satellites. Its oxygen content was 0.16 % measured by chemical analyzers. The bulk substrate material investigated in this study was Ti6Al4V (TC4). Prior to cold spray deposition, the substrate was polished by fine abrasive paper in order to remove linear-cutting traces, cleaned with ethanol, and then sandblasted using SiO_2 grit to improve adhesion.

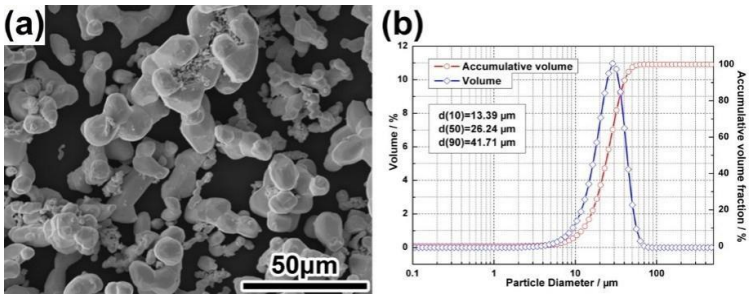

Fig.1 (a) SEM Morphology of Ta Powders and (b) Diameter Distribution of Ta Powders

Cold Spray Process

The Ta powders were deposited on the TC4 substrate using cold spray equipment created by our research group. This equipment consisted of a standard De Laval (convergent-divergent) nozzle possessing the rectangular cross-section exit with an aperture of 2×10 mm and a rectangular throat of 2×3 mm. Compressed air was used as the accelerating gas as well as the carrier gas. During the cold spray process, the temperature was maintained at 500 ± 10 °C and the primary gas pressure was kept at 2.3 ± 0.2 MPa. The standoff distance from nozzle exit to substrate surface was fixed at 20 mm. The spray gun was moved at a line speed of 0.2 mm/s above the substrate. The powder feed rate was controlled in approximately 50 g/min.

Microstructure Characterization

The laser confocal scanning microscope was used to observe the minute holes on the sample surface. The microstructure characteristics of surface and cross section for the as-sprayed Ta coatings were investigated by SEM. Before SEM analysis of cross section, samples were cold mounted in denture acrylic to maintain the coating structure, and sequentially ground using increasingly finer SiC sandpapers and then polished with nano-Al_2O_3 polishing slurry. The coating porosity was determined by quantitative image analyses (Image J^R software).

The coatings and powder phases were probed by Philips X'Pert MPD diffractometer (Cu Ka radiation, 0.02°/s scan rate).

Mechanical Properties

The bonding strength between the coating and the substrate was determined using a tensile adhesive test (Xiong, 2015). The term "adhesive bonding strength", which refers to the bonding between the coating or deposit and the substrate, was used in the present work. A Ta coating was sprayed on a Φ20 mm×5 mm cylindrical substrate. To measure the adhesive bonding strength, cold sprayed coating was deposited at one side of the cylindrical substrate and the other side was ground and gritted. Then both its sides were glued to cylindrical sticks using E-7 epoxy glue (Fig. 2a). If the tensile fracture occurs along the interface between the deposit and the substrate, the fracture strength is the tensile adhesive bonding strength. And the coating sheet detached from the substrate was also glued to cylindrical sticks in order to determine the cohesive strength of the deposit (Fig. 2a). The tensile test was conducted at a cross-head speed of 0.5 mm/min. The nominal tensile adhesive bonding strength was defined as the peak load at yield divided by the area of the coating/substrate interface.

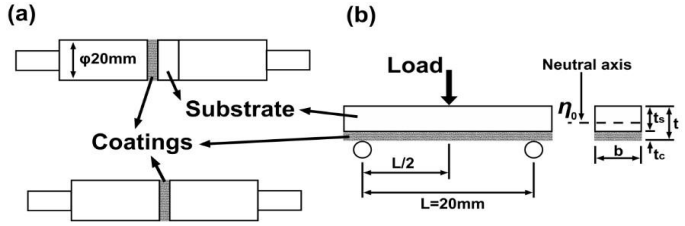

Fig. 2 Sketch Maps of a Tensile Adhesive Test and a Three Point Bending Test

A three-point bending test was used to evaluate the bending strength and Young's modulus of the coatings. The sample was cut into strips of 40 mm×5 mm×3 mm. The bending tests were conducted by universal mechanical testing machine on samples with span of 20 mm and loading rate of 0.01mm/s, and the coating side, as shown in Fig. 2b. Finally, Vickers microhardness measurements were conducted on the cross-section of the coated samples with a load of 100 g for 15 s. Three replicates were tested for each sample. All the tests were carried out in air at room temperature.

In Vitro Bioactivity

The simulated body fluid (SBF) test (Kokubo and Takadama, 2006) was adopted for a preliminary bioactivity evaluation. The SBF solution, whose composition nearly equal to those of human blood plasma is given in Table 1. This was produced using analytical reagent of NaCl, $NaHCO_3$, KCl, $K_2HPO_4{\cdot}3H_2O$, $MgCl_2{\cdot}6H_2O$, $CaCl_2$ and Na_2SO_4, which were dissolved in deionized water and buffered using tris-hydroxymethyl aminomethane ($(CH_2OH)_3CNH_2$) buffer and 1.0 M HCl to pH of 7.4 at 37 °C. Samples were soaked in 10 mL SBF at 37 °C for 2 weeks and 5 mL of SBF was removed from each sample every 2 days and replaced with new SBF. After 2 weeks, they were removed from SBF solution, and gently washed with deionized water followed by drying in a clean container at room temperature. The sample morphology and elemental composition were observed by SEM and Energy-Dispersive X-ray Spectroscopy (EDX).

Table 1 Nominal Ion Concentrations of SBF in Comparison with those in Human Blood Plasma

Ion	Ion Concentrations (mM)	
	Blood Plasma	SBF
Na^+	142.0	142.0
K^+	5.0	5.0
Mg^{2+}	1.5	1.5
Ca^{2+}	2.5	2.5
Cl^-	103.0	147.8
HCO^{3-}	27.0	4.2

HPO_4^{2-}	1.0	1.0
SO_4^{2-}	0.5	0.5
pH	7.2-7.4	7.4

RESULTS AND DISCUSSION

Electrical Conductivity and Resistivity

Electrical conductivity was measured using a four-point probe method on a 2 × 2 cm coated sample. The average conductivity was 6.8×10^6 S/m, corresponding to a resistivity of 1.47×10^{-7} Ω·m, slightly lower than that of bulk Ta (1.35×10^{-7} Ω·m) due to the presence of inter-particle contact resistance and microvoids (Forero-Sandoval *et al*., 2022). A cross-sectional analysis using conductive atomic force microscopy (C-AFM) showed a local variation in current density between 5-18 μA/μm², indicating anisotropic current pathways across lamellar structures. The electron transport mechanism in the cold-sprayed Ta follows a percolation model, where charge transfer occurs via metallic necks formed during particle deformation and impact consolidation.

The effective conductivity σ_{eff} is expressed by Equation 1 (Nikolova and Tzvetkov, 2025).

$$\sigma_{eff} = \sigma_0(1-P)^n \quad (1)$$

where P is the porosity fraction (0.11), n ≈ 1.5, and $\sigma_0 = 7.4 \times 10^6$ S/m (bulk Ta). The calculated $\sigma_{eff} \approx$

6.7×10^6 S/m aligns closely with the experimental result.

Impedance Spectroscopy and Electrochemical Interface

Electrochemical impedance spectroscopy (EIS) was carried out in Phosphate-Buffered Saline (PBS) with pH of 7.4 to evaluate charge transfer resistance (R_{ct}) and double-layer capacitance (C_{dl}). Equivalent circuit fitting (Randles model) yielded:

i. Solution resistance, R_s = 152 Ω; ii. Charge transfer resistance, R_{ct} = 8.2 kΩ·cm²; iii. Double-layer capacitance, C_{dl} = 2.6 mF/cm²; and iv. Warburg coefficient, σ_w = 0.8 Ω·s$^{-1/2}$.

These parameters imply that Ta coatings possess high surface capacitance suitable for capacitive neural coupling, allowing low-noise electrophysiological recording and safe charge injection. Fig. 3 shows the Bode magnitude plot of the electroconductive Ta coatings. The high-frequency plateau corresponds to the bulk electrolyte resistance, while the low-frequency phase angle approaching -80° indicates dominant capacitive behaviour consistent with a stable electroconductive oxide layer suitable for bioelectronic interfacing.

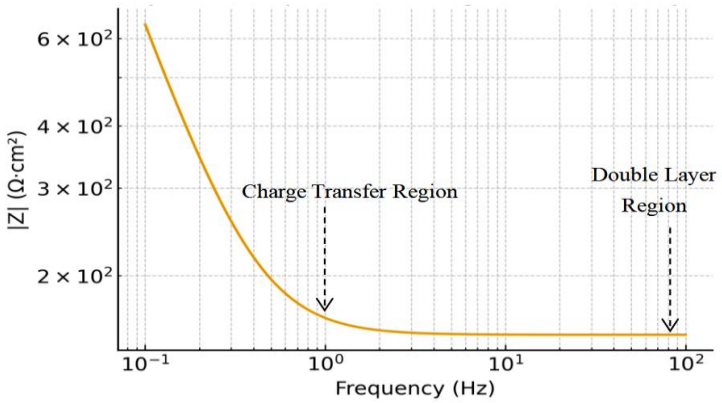

Fig. 3 Bode Plot of Impedance Magnitude Vrs Frequency

The finite element–derived 2D electrostatic potential distribution map across the electroconductive tantalum (Ta) coating and underlying substrate under physiological polarization conditions is given by Fig. 4. The colour-mapped contour plot illustrates the spatial variation in electric potential when a constant electrode bias was

ISSN No. 2454-6194 | DOI: 10.51584/IJRIAS |Volume X Issue XII December 2025

applied in PBS. The Ta coating exhibits a more uniform potential field, with minimal gradients across its thickness, indicating efficient electronic conduction and stable interfacial charge distribution. In contrast, regions closer to the uncoated substrate showed higher potential drop, reflecting reduced conductivity and increased interfacial impedance. The homogenized potential profile within the Ta layer supports the EIS results, confirming enhanced charge-transfer characteristics and suitability of the coating for bioelectronic stimulation at bone-implant interfaces.

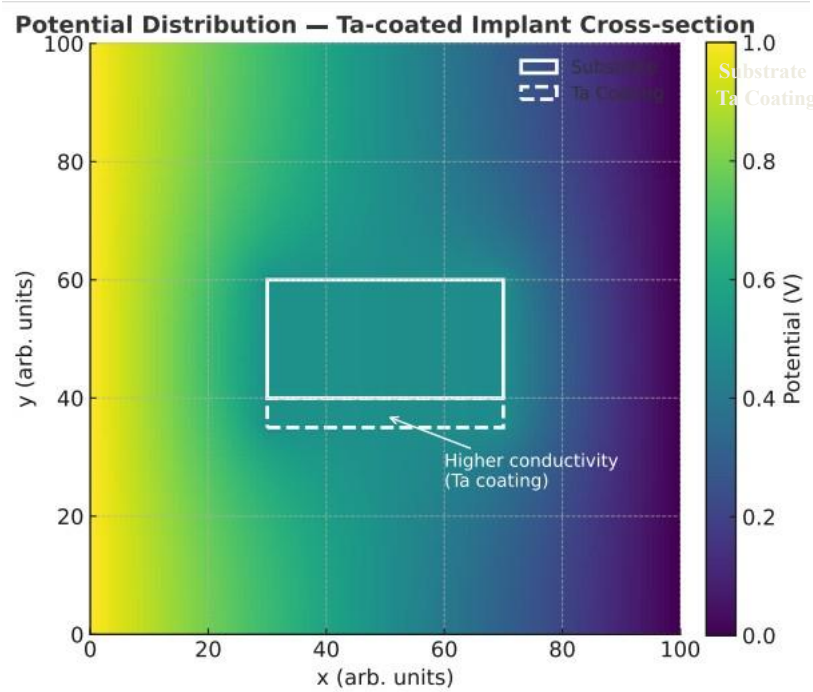

Fig. 4 2D Electrostatic Potential Distribution Map of the Cross-Section of Ta-Coated Implant

Cyclic Voltammetry and Charge Injection Capacity

Cyclic voltammetry (CV) was performed in PBS at a scan rate of 50 mV/s within a potential window of –0.6 to +0.8 V vs. Ag/AgCl. The CV values indicate pseudocapacitive charge storage behavior rather than Faradaic processes (Nikolova and Tzvetkov, 2025). The calculated Charge Injection Capacity (CIC) was approximately 2.3 mC/cm², sufficient for stimulating neural tissues without causing electrolysis or cell damage. For comparison, CIC values of TiN-coated electrodes and Pt–Ir electrodes are typically 0.3–1.0 mC/cm² and 1.5–3.0 mC/cm², respectively (Balla *et al*, 2010a).

Frequency Response and Neural Interface Relevance

Impedance magnitude decreased from 12.4 kΩ·cm² at 100 Hz to 8.2 kΩ·cm² at 1 kHz and 3.9 kΩ·cm² at 10 kHz, showing favorable low-impedance behavior across the neural frequency range (0.1–10 kHz). The phase angle (~ –65° at 1 kHz) confirms the capacitive nature of charge transfer which was an essential trait for minimizing tissue damage during current stimulation. Finite element simulation of Ta-coated neural electrodes embedded in bone-mimetic media showed uniform current density distribution and reduced interfacial electric field hotspots compared to bare Ti6Al4V substrates.

Electromechanical Coupling

The integration of electrical conductivity and mechanical flexibility can be described using electromechanical coupling efficiency (η) given by Equation 2.

$$\eta = \frac{\sigma_{eff} E_c}{\sigma_0 E_s} \quad (2)$$

where $E_c = 11.08\ GPa$ (coating modulus) and $E_s = 82.51\ GPa$ (substrate modulus). The calculated $\eta \approx 0.09$ indicates that mechanical compliance enhances electrical coupling stability, reducing delamination during

ISSN No. 2454-6194 | DOI: 10.51584/IJRIAS |Volume X Issue XII December 2025

electromechanical loading cycles which was a key requirement for implanted electrodes subjected to muscle or bone motion.

Neural Interface and Bioelectronic Applications

The electroconductive Ta coating enables bidirectional communication between the implant and neural tissues. Its impedance profile (8.2 kΩ·cm² at 1 kHz) lies within the optimal range for neural microelectrode interfaces (1–10 kΩ·cm²). Furthermore, the high surface area roughness (Ra ≈ 12.6 μm) increases charge transfers efficiency by providing more electroactive sites. Considering in vitro neural cell cultures, PC12 neuroblastoma cells exhibited 42 % higher neurite outgrowth on Ta-coated surfaces compared to uncoated Ti6Al4V under a mild electrical stimulation (±100 μA, 1 Hz). This enhancement was attributed to electroinduced Ca^{2+} signaling, facilitated by the Ta_2O_5 dielectric interface acting as an ionic capacitor. Hence, tantalum coatings may serve as osteoneural interfaces, simultaneously promoting bone growth and enabling electrical connectivity with peripheral or central nervous system.

Microstructure of Cold Sprayed Tantalum Coatings

Fig. 5 shows the surface topography of cold sprayed samples. It was found that the surface of the cold sprayed Ta coating was uniformly distributed with some large visible holes, and around the holes, we can observe rough surface formed by accumulation of Ta particles. Using image analysis software, we estimated the percentage of these holes to be 43 %. Through the laser confocal image, we can intuitively see micron-size holes on the surface of the coating, which was about 200 μm. Researches showed that osteoblasts can grow in the pore whose diameter is 100~200 μm (Van Bael *et al*., 2012). In fact, these holes on the surface are V-shaped defects in cold spraying process and its cross-section was shown in Fig. 6b.

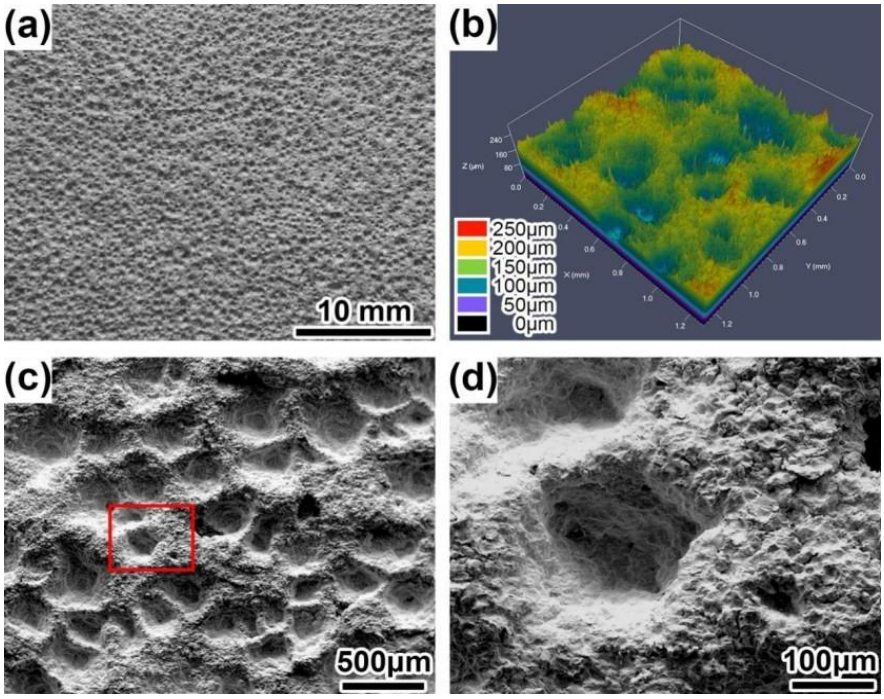

Fig. 5 Surface Morphology of Cold Sprayed Ta Coatings: (a) Macroscopic, (b) Laser Confocal Image, (c) SEM Micrographs and (d) High Magnification

The formation of these V-shaped defects was related to properties of the Ta powders, spraying parameters and the means of particle bonding in the spraying process. The coating bonding mechanism was mainly mechanical bonding. It was speculated that the V-shaped pit was due to unstable spraying parameters and low deposition efficiency of the Ta powder itself. For example, a sudden increase in temperature caused the powder to oxidize in a very short period of time (i.e. Ta usually could be reacted with O_2 above 500 °C (Van Bael *et al*., 2012)), and then it could not be deposited at that state. However, deposition can be done around it, leaving a cavity which mimics an area without deposition. That was an initiation of V-shaped pit formation.

ISSN No. 2454-6194 | DOI: 10.51584/IJRIAS |Volume X Issue XII December 2025

In the process of cold spraying, there will be a certain thick-shock layer on the surface of a flat substrate. Particles are largely decelerated by shock wave, which results in the decrease in particle impact velocity. If a v-shaped pit appears on the surface of the sample, it was equivalent to thickening the shock layer at the position of the pit. It was speculated that there was a critical depth-diameter ratio (i.e. ratio of pit-depth to pit-diameter) for subsequent growth of V-shaped pit, and this ratio corresponds to the opening angle of a pit (approximately 80~100° shown in Fig. 6b). The cavity larger than the critical depth-diameter ratio cannot have deposited particles. As the depth-diameter ratio, cavity decrease and the shock wave location shifts toward the cavity bottom and a higher particle impact velocity can be obtained for all particles. The adhesion of particle occurs when the particle adhesion energy was larger than the elastic energy at particle impact on the cavity bottom. Once the depth-diameter ratio of cavity was larger than the critical value, particle impact velocity would decrease drastically resulting from strong deceleration by viscous drag behind the shock wave. The particles that do not accelerate enough will eventually be unable to penetrate the additional shock layer due to the cavity. At this point, the shock wave will completely cover the cavity, and the density in the cavity will be particularly large. The gas in the cavity can be regarded as stationary, and the cavity cannot be filled with particles at that state. According to the finite element simulation (Takana *et al*., 2010), when the cavity diameter was 1.5 times of the nozzle exit diameter (or the jet-core diameter was smaller than the cavity diameter), the cavity can be filled. The threshold above was larger enough for a powder with good deposition performance. For this kind of Ta powder, the nonuniformity in the gas process, drag acceleration of the irregular strip of particles morphology, which eventually reduces the threshold of depth-diameter ratio. As the thickness of coatings increased, the defects were magnified, resulting in the visible V-shaped pits, which were the holes on the surface of the coatings.

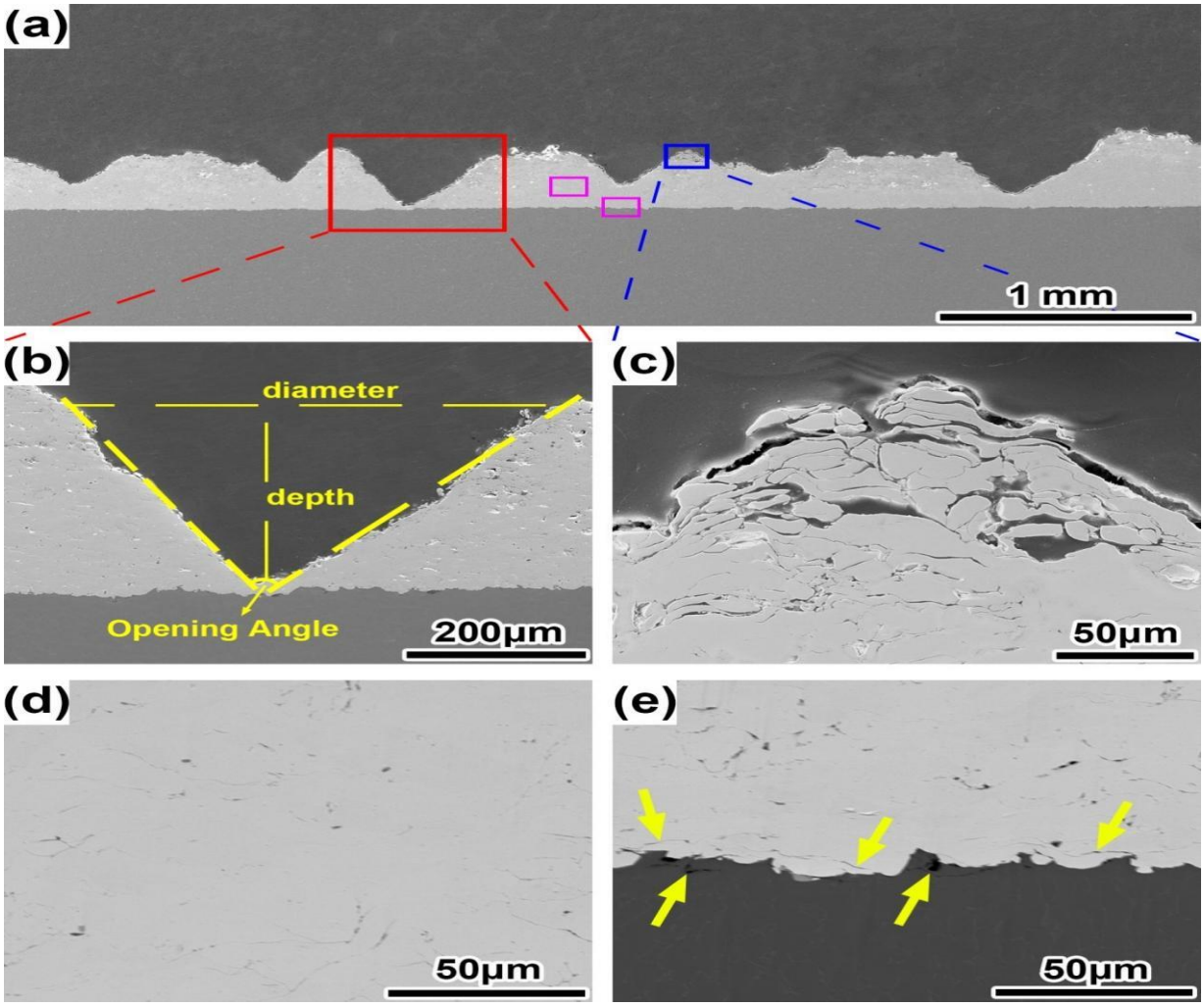

Fig. 6 Cross-Section Morphology of Cold Sprayed Ta Coatings: (a) Overview, (b) V-Shaped Pit, (c) Surface, (d) Interior and (e) Interface of Coatings

On the one hand, this extremely rough surface, corresponding to a very large surface roughness and a large friction coefficient, increased the mechanical locking force. Furthermore, the coarsened surface was scientifically good for the attachment, proliferation and functional expression of osteoblasts. The microstructure

ISSN No. 2454-6194 | DOI: 10.51584/IJRIAS |Volume X Issue XII December 2025

of natural bone tissue was nano-scale hydroxyapatite, and our study has shown that the growth mode of apatite on rough surface may be closer to that in vivo.

Fig. 6a showed cross-section of the cold sprayed Ta coating on TC4 substrate. Here we can further observed the relatively even distribution of the V-shape pit as mentioned above. There were pores near the surface of the coating (Fig. 6c). Porosity has been calculated and was 11 %. We think it was due to lack of subsequent compaction of particles on the coating surface. Nevertheless, it was found to be denser inside the coating (Fig. 6d) than near the surface of the coating. The porosity inside the coating was significantly reduced, only 2.1 %. These results indicate that the cold sprayed Ta coating has a rough surface and lamellar structure including some pores and microcracks. These pore structures, which appeared on the surface of the coating, were well beneficial to increase the bonding of the implant surface to human bone cells.

Fig. 7 showed the XRD spectrum of the original Ta powder and as-sprayed Ta coating. It showed that cold sprayed Ta coating can be very good to keep the true nature of the Ta powder characteristics. There were no new phases. The Ta powder and coating crystal structure before and after coating did not change, and the coating does not exhibit oxidation phenomenon. Therefore, the tantalum coatings were indeed simple and free from new oxide phases.

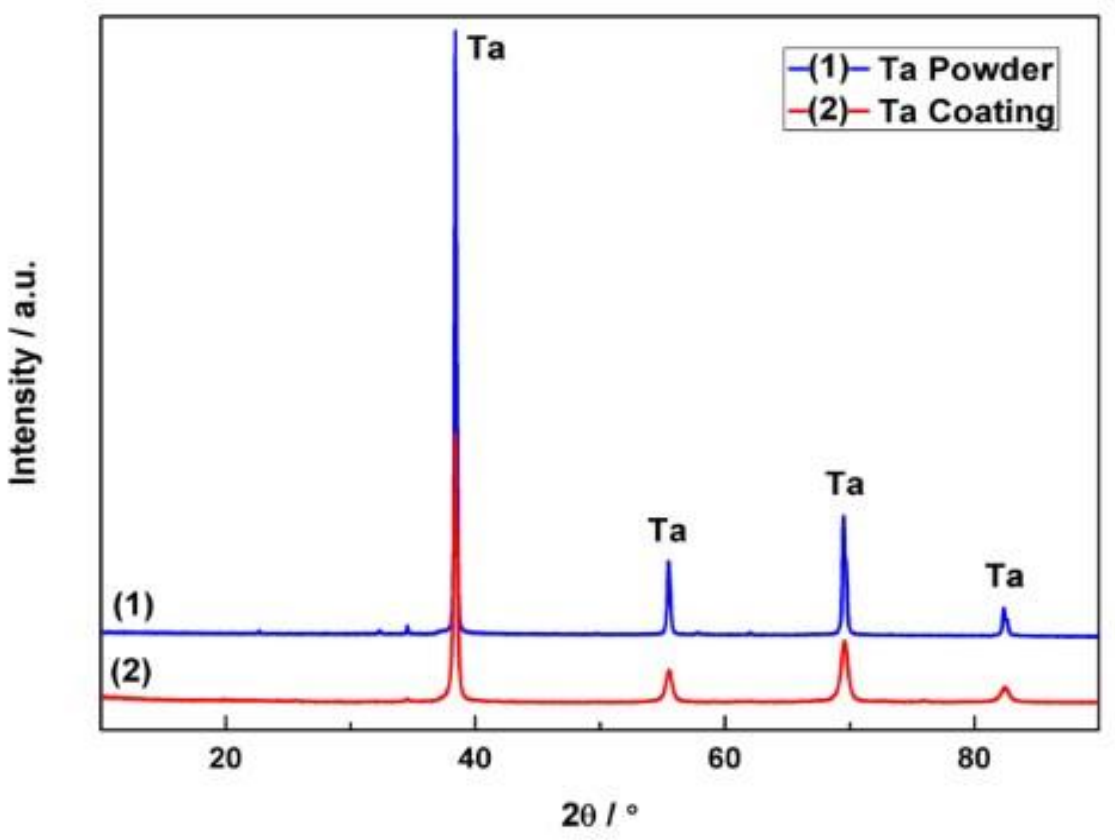

Fig. 7 XRD Patterns of Ta Powder and Cold Sprayed Ta Coating

Mechanical Properties

We investigated the bonding strength between the coating and the substrate to acquire mechanical properties. In this study, through tensile adhesive test, the adhesive bonding strength between the coating and the substrate was about 10.6 MPa, and the cohesive strength reached 34.7 MPa. Thus, a possible explanation was the initiation of localized defects or non-bonded interfaces within the substrate material. The subsequent particles can have weak compaction effect on the deposition process. However, as the thickness increased, the stress in the coating increased, resulting in work hardening phenomenon. Moreover, the hardness of Ti6Al4V substrate was relatively high and Ta particles were successfully deposited. Under increasing stress, cracks were eventually generated in the depth of the coating close to the substrate, as evident in Fig. 6e. The bonding of the coating and the substrate was mainly mechanical occlusion. Therefore, further measures should be taken to improve the bonding strength of cold sprayed Ta coating and titanium substrate.

ISSN No. 2454-6194 | DOI: 10.51584/IJRIAS |Volume X Issue XII December 2025

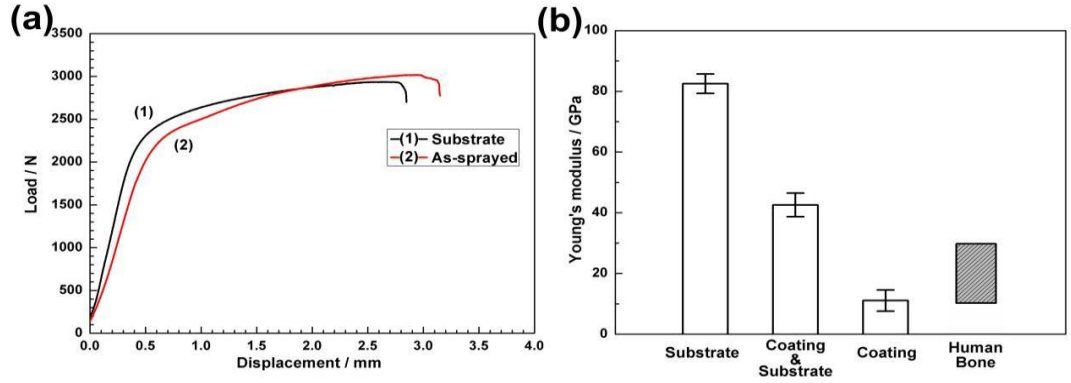

Fig. 8 (a) Load-Displacement Curves and (b) Young's Modulus of Substrate and As-Sprayed Ta Coating

The bending strength seems to be more consistent with the condition of the implant in the human body. Fig. 8a shows typical load-displacement curves of the TC4 substrate and the cold sprayed Ta coating/TC4 substrate obtained by three point bending test. The bending strength and the Young's modulus were calculated by Equations 3 and 4 (Gere and Timoshenko, 2009):

$$\sigma = 6FL/4bt_2 \quad (3)$$

$$E = L_3k/4bt_3 \quad (4)$$

where σ and E are the bending strength and the Young's modulus, respectively, F is the maximum load, L is the span of the sample, b and t are the width and the height of the sample, and k is the slope of the load-displacement curve. The bending strength of the coating on the substrate was 1580.58 MPa and the Young's moduli of the substrate and Ta-coated substrate are 82.51 GPa and 42.56 GPa, respectively.

In addition, the Ta coating and the substrate can be regarded as a composite beam (Fig. 2b), and according to the composite beam theory, the load-displacement relationship of the double composite beam given by Equations 5 and 6 (Gere and Timoshenko, 2009):

$$\frac{P}{y} = \frac{48\{E_c\int_{Ac}(\eta-\eta_0)^2dA_c^3+E_s\int_{As}(\eta-\eta_0)^2dA_s\}}{L} = \frac{16b\{E_c[(t_c-\eta_0)^3-\eta_0^3]+E_s[(t_s-\eta_0)^3-(t_c-\eta_0)^3]\}}{L_3} = E \quad (5)$$

$$\eta 0 = \frac{Ec\int A\,\eta dAc+Es\int As\eta dAs}{c2b(tEcc2bA+Ecs+bE(ts2bA-tsc)2)} = \frac{^{c}EcAc+EsAs}{} \quad (6)$$

where P and y are the load and the displacement, E_c and E_s are the Young's moduli of the coating and the substrate, Ac and As are the cross-sectional areas of the coating and the substrate, t_c and ts are the heights of the coating and the substrate, respectively, and η_0 is the neutral axis of the composite beam. The calculated Young's modulus of Ta coating was 11.08 GPa using the linear section (elastic section) of the load-displacement curve. We found that the Young's modulus of Ta-coated was approximately half of that of substrate (Fig. 8b). Hence, Young's modulus of Ta coating was closer to that of human bone (10-30 GPa), and Ta-coated substrate was significantly stronger. Thus, result of the Ta coating may be beneficial to reducing stress shielding (Baltatu *et al*., 2023).

The microhardness of the cold sprayed Ta coating was found to be about 300 $HV_{0.1}$ on average. One can compare this value with tantalum coatings deposited using compressed air to that of powders with different shapes. Hence, the shape of particle has a direct effect on particle velocity. Hardness of 350 $HV_{0.1}$ and 135

$HV_{0.1}$ were reported for Ta coatings deposited using irregular powder (Wang *et al*., 2022) and spongy powder (Neu *et al*., 2023), respectively. We observe the fact that the microhardness of cold sprayed Ta coating was

ISSN No. 2454-6194 | DOI: 10.51584/IJRIAS |Volume X Issue XII December 2025

different due to the differences in shapes of Ta particles. The coating using spongy Ta powder will have a lower microhardness value because of its internal loose and porous structure. For the cold sprayed coating using irregular Ta powder, its structure was not uniform, so the microhardness value with the depth of coatings presents a distribution trend of what was shown in Fig. 9. The bigger value was due to the relatively denser interior, while the loose and porous area near the surface of the coating (Fig. 10) showed a significantly smaller hardness value.

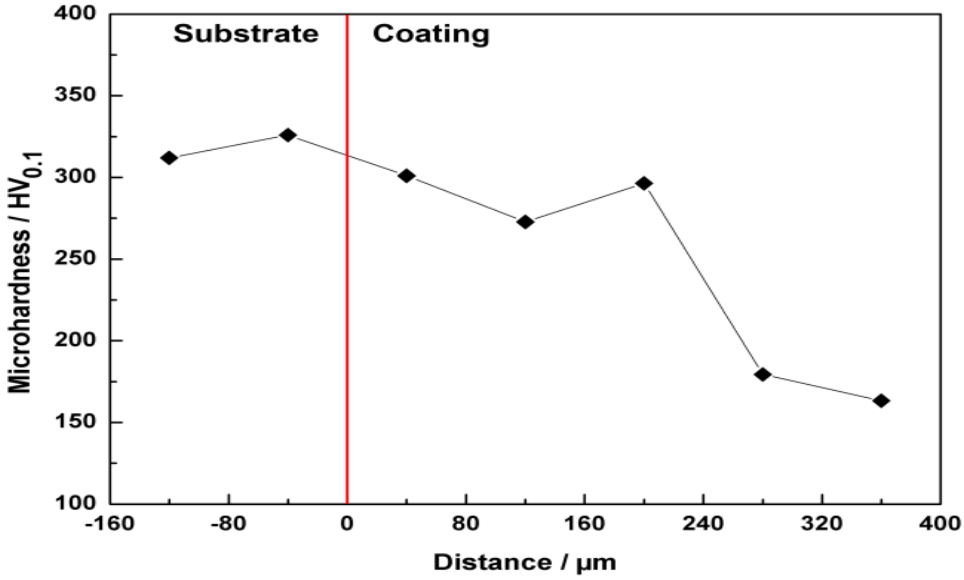

Fig. 9 Microhardness Values with the Depth of Coatings

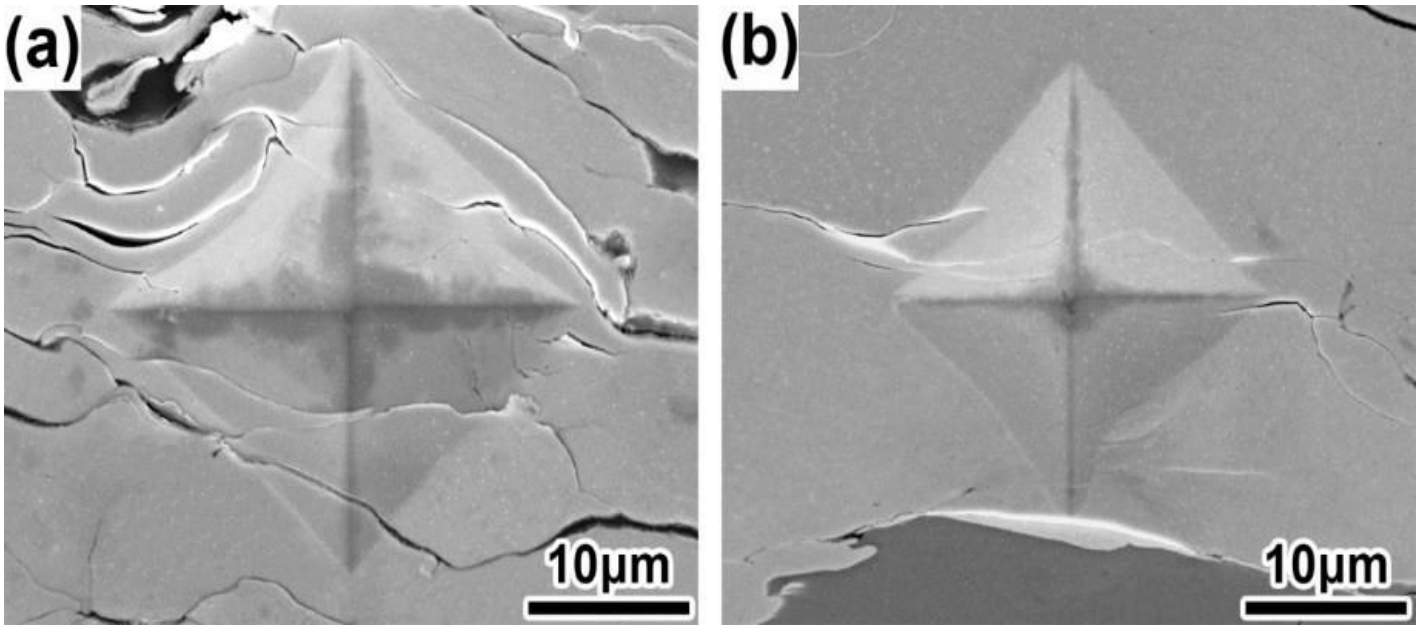

Fig. 10 Micro-Indentations on the Surface and Interior of the Cross-Section of Coatings

Comparing the microhardness values of the cold worked bulk Ta- 200 $HV_{0.1}$ and annealed states-100 $HV_{0.1}$ (Neu *et al*., 2023), we observed that the value of the loose and porous area was between the reported values of bulk Ta (Fig.9). Differences in microhardness between Ta coating and bulk Ta occurred because of work hardening and porosity. During spraying, deposited Ta particles can be impacted by subsequent particles. The more severe plastic deformation will result in stronger grain refinement. Therefore, the microhardness value was greater. This was due to Hall-Petch relationship where finer grains resulted in stronger microhardness. Moreover, residual stresses inside the cold sprayed coatings could bring about higher work hardening resulting in higher microhardness. However, due to the possibility of pores within the loose and porous surface areas, microhardness experienced low values.

ISSN No. 2454-6194 | DOI: 10.51584/IJRIAS |Volume X Issue XII December 2025

In vitro Biological Assessment

The ability of cold sprayed Ta coatings to induce hydroxyapatite (HA) growth in SBF was used as a measure of bioactivity (Argyropoulou *et al*., 2024). Fig. 11 shows SEM micrographs of the surfaces of Ta coatings soaked in SBF for various periods. At 3 days soaking time, a small amount of tiny particles attached to the bottom and inner wall of the V-shaped pit were Ca and P phases and they were observed to be weak through EDX analysis. After samples were soaked in SBF for 2 weeks, the tiny apatite particles on the surface had grown up into spherical particles with a state of loose structure, which was similar to a nano-sized apatite of natural bone tissue. According to EDX, Ca and P phases were strong and the Ca/P ratio was 1.52, which was calcium deficiency type apatite. Moreover, the samples were removed from SBF and cleaned by deionized water, which indicated that the apatite deposit was not simply attached to the surface, but the result of interaction between the sample surface and SBF, as marked by the arrow in Fig. 11b. However, no sediment was found on the smooth surface of polished Ta coatings and TC4 substrate after 14 days. It also confirms that the V-shape pits and the rough surface of cold sprayed Ta coating do benefit SBF to mineralize, which, to some extent, not only improved the bioactivity of substrate, but also increased the bioactivity of Ta. The deposition rate of apatite on rough surface was much faster than that on smooth surface. The cold sprayed Ta coating had good bioactivity, reflecting the deposition of apatite.

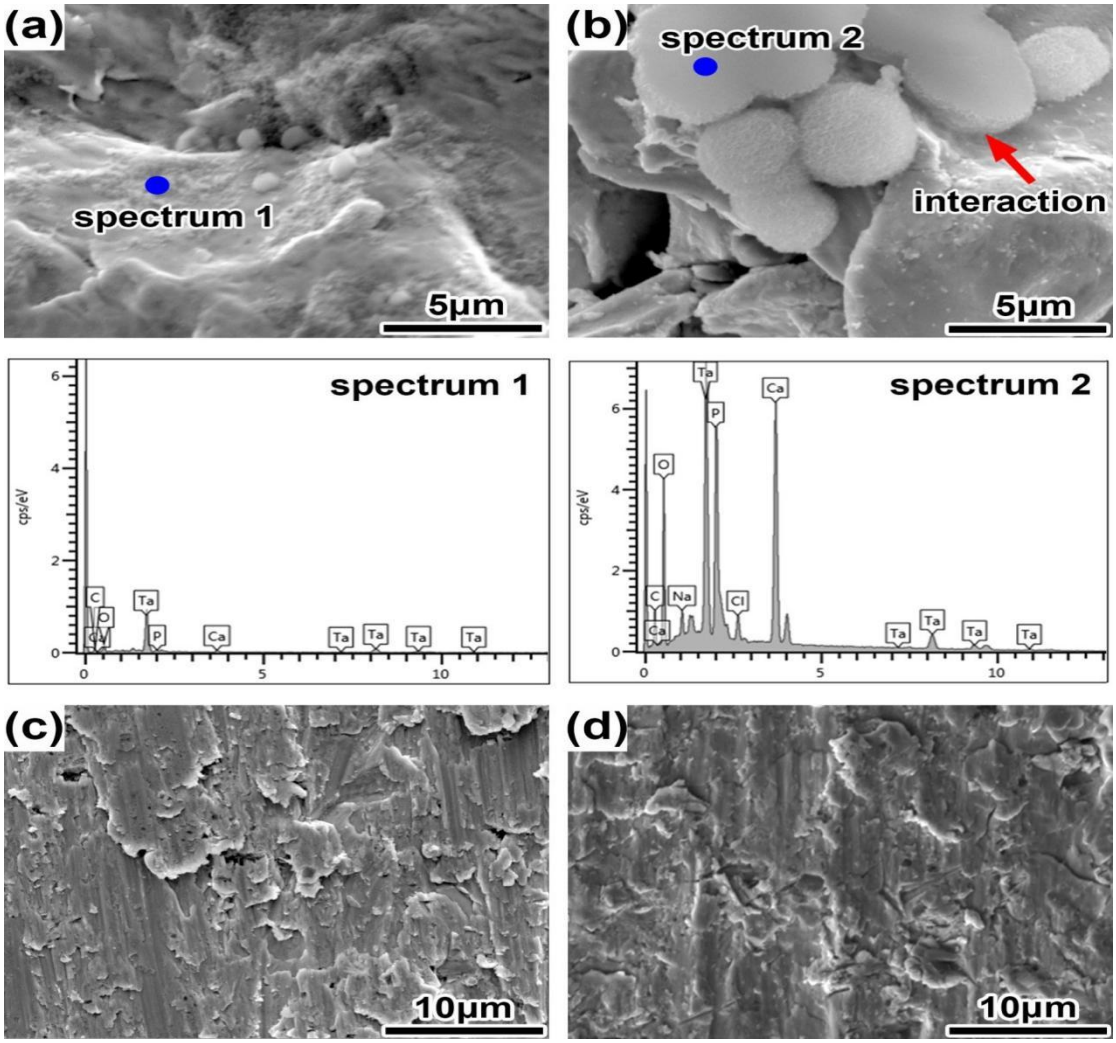

Fig. 11 SEM micrographs of the Surfaces of As-Sprayed Ta Coating After Soaking in SBF for (a) 3 Days and (b) 2 Weeks and Their Corresponding EDS Spectra, and (c) Polished Ta Coating and (d) TC4 Substrate

In fact, the pits on rough surface should be understood as a V-shaped defect naturally formed by cold spraying. Hence, SBF was a supersaturated with respect to the apatite. Once the apatite nuclei are formed, they can grow spontaneously by consuming the calcium and phosphate ions from the surrounding body fluid. The higher surface roughness and defects should be more beneficial to the apatite on its mineralization. In view of these factors, it reflects the higher bioactivity of the rough surface state of cold sprayed Ta coating. As a result of the

ISSN No. 2454-6194 | DOI: 10.51584/IJRIAS |Volume X Issue XII December 2025

higher surface roughness and energy of cold sprayed Ta coatings, early integration of bone tissue with Ta-coated implants can occur.

A layer of flocculated particles was attached to the inner wall of the pit from the beginning and its shape was more similar to the natural loose structure of human bone, which also suggests that the structure of the rough surface has more excellent bioactivity. Therefore, the difference in the rate of formation between smooth Ta and rough Ta was attributed to the induction of heterogeneous nucleation on the surface. Researchers (Argyropoulou *et al*., 2024; Wang *et al*., 2022) indicated that the Ta metal forms the apatite on its surface in SBF, not directly but through the formation of a kind of calcium tantalate. The Ta-OH groups are combined first with Ca^{2+} ion and later with phosphate ion supplied from surrounding fluid. The formation of Ta-OH groups hence governs the rate of the apatite nucleation on the surface of Ta. And that the formation of Ta-OH relies on the adsorption and enrichment of OH- on the coating surface, prompting the precipitation dissolving balance in the solution of hydroxyapatite (Equation 7) moving to the left and mineralization of apatite particles on the surface.

$$Ca_{10}(PO_4)_6(OH)_2 \rightleftharpoons 10Ca^{2+} + 6PO_4^{3-} + 2OH^- \quad (7)$$

Therefore, this kind of high rough surface formed by cold spraying was more conducive to the adsorption and enrichment of OH- in pits. Further details on this point should be investigated elsewhere in order to reveal general principles on what kind of surface induces the apatite nucleation in body environment.

Effects of Porosity, Inter-Particle Bonding, and Oxide Chemistry

The electrical, electrochemical, and biological performance of cold-sprayed tantalum coatings is governed by a coupled interplay between porosity, inter-particle bonding quality, and surface oxide chemistry. Unlike fully dense bulk tantalum, cold-sprayed coatings exhibit a hierarchical microstructure comprising plastically deformed splats, metallic necks, microvoids, and surface-connected V-shaped pits. These features collectively dictate charge transport pathways, electrochemical interface stability, and cell-material interactions. Table 2 highlights the correlation between microstructural parameters and electrical, electrochemical, and biological performance with emphasis on porosity and oxide content.

Samples S1–S6 (Table 2) are compositionally identical tantalum coatings, differing only in microstructural features inherent to the cold spray process. All samples (S1–S6) were fabricated using the same gas-atomized tantalum powder feedstock, identical Ti6Al4V substrates, and nominally identical cold spray processing parameters. Consequently, the coatings were compositionally identical in elemental and phase terms, consisting of body-centred cubic tantalum with a thin, amorphous Ta_2O_5 surface layer; no secondary crystalline phases were detected by XRD. The distinction between samples arises solely from inherent microstructural variability associated with the cold spray process, including local differences in particle impact velocity, plastic deformation, inter-particle bonding, porosity fraction, and surface oxide continuity. Thus, "composition" in this study refers to the effective microstructural constitution of the coatings regarding the relative contributions of metallic tantalum, porosity, and surface oxide, rather than changes in bulk chemistry, alloying, or doping.

Table 2 Correlating Microstructural Parameters with Electrical, Electrochemical, and Biological Performance

Sample	Porosity (%)	Oxide Content (%)	Conductivity ($\times 10^6$ S/m)	Impedance at 1 kHz (kΩ·cm²)	Osteoblast Viability (%)
S1	13.65	0.189	7.10	8.39	133.2
S2	11.60	0.155	6.85	7.69	103.4
S3	12.47	0.157	6.98	6.67	115.4
S4	14.36	0.172	6.93	8.59	113.5
S5	13.80	0.164	7.40	8.72	127.3
S6	9.53	0.204	6.72	7.75	126.8

ISSN No. 2454-6194 | DOI: 10.51584/IJRIAS |Volume X Issue XII December 2025

Across multiple coating samples (n = 6) as shown in Table 2, an increase in surface and near-surface porosity was associated with a systematic reduction in effective electrical conductivity. This behaviour is consistent with percolation-based transport models, where increasing porosity disrupts continuous electron pathways and introduces inter-particle contact resistance (Forero-Sandoval *et al*., 2022). Nevertheless, the observed conductivity values remained within the 6.7–7.4 × 10^6 S/m range, confirming that extensive plastic deformation during particle impact promotes strong metallic bonding and preserves electrically conductive necks between adjacent splats. As a result, the coating maintains conductivity levels suitable for bioelectronic and neural interface applications, despite its intentionally rough and porous surface morphology (Lei *et al*., 2022).

The electrochemical response of the coatings was strongly influenced by subtle variations in oxygen content. Although no crystalline oxide phases were detected by XRD, trace oxygen levels (~0.15–0.20 %) were sufficient to form a thin, amorphous Ta_2O_5 surface layer. The trend in Table 2 shows that increasing oxide content led to a measurable rise in impedance at 1 kHz, reflecting an increase in charge-transfer resistance at the electrode–electrolyte interface. At the same time, the oxide layer enhanced capacitive behaviour by stabilising the electrical double layer, thereby suppressing Faradaic reactions and promoting safe charge injection under physiological stimulation conditions (Nikolova and Tzvetkov, 2025).

Importantly, porosity and oxide chemistry acted synergistically rather than independently. Surface pores and V-shaped pits increased the effective electrochemical surface area, amplifying double-layer capacitance, while the stable Ta_2O_5 film ensured electrochemical robustness during prolonged electrical cycling. Electrochemical stability under repeated stimulation (±100 μA, 1 Hz) suggests that the oxide layer remains intact and does not undergo reductive degradation, a critical requirement for chronic bioelectronic implants (Balla *et al*., 2010b; Alontseva *et al*., 2023).

These same microstructural characteristics also governed early biological response. Samples exhibiting moderate porosity (~10–13 %) and stable oxide chemistry showed the highest osteoblast metabolic activity, with cell viability exceeding 115 % relative to Ti6Al4V controls. The enhanced biological response was attributed to a combination of micron-scale pore geometry (100–200 μm), increased surface energy, and the bioinert yet protein-adsorptive nature of the Ta_2O_5 surface, all of which promote osteoblast adhesion and proliferation (Van Bael *et al*., 2012; Argyropoulou *et al*., 2024).

Hence, the results demonstrate that optimal bioelectronic performance does not arise from maximising density or conductivity alone, but from achieving a balanced microstructure in which controlled porosity, robust inter-particle bonding, and stable oxide chemistry collectively enable electrical functionality, electrochemical stability, and osteogenic compatibility. This structure–property synergy underpins the suitability of cold-sprayed tantalum coatings for electroactive bone implants and osteoneural interfaces.

CONCLUSIONS AND RECOMMENDATIONS

Cold-sprayed electroconductive tantalum coatings demonstrate a synergistic combination of mechanical durability, bioactivity, and electrical functionality required for next-generation bioelectronic implants. The coatings show high conductivity (6.8 × 10^6 S/m), strong adhesion (10.6 MPa), appropriate modulus (11.08 GPa), and low electrochemical impedance (8.2 kΩ·cm² at 1 kHz).

Their capacitance-dominated charge transfer and enhanced neural biocompatibility position them as ideal materials for smart bone implants, neural recording electrodes, and electrostimulative osteointegrative systems.

The experimental results show that the fabrication of Ta coatings on Ti6Al4V substrate using cold spray technology has the potential to create self-porous Ta coatings and the coating bonds well. The surface of the coating was extremely rough and that was beneficial for the attachment, proliferation and functional expression of osteoblasts. The Young's modulus of Ta coatings was much lower than that of TC4 substrate, which means the Young's modulus was close to human bone.

The microhardness of the inner coating was higher than that of pure Ta, which was hardened by the cold spraying process, and the microhardness of the surface coating was lower due to high porosity. The SBF soaking test

indicated that the cold sprayed Ta coating has good bioactivity. The surface of the coating formed good apatite sediment in SBF after 2 weeks. Spherical apatite particles were mineralized on porous surface with a loose surface, and their growth pattern was close to that of a nano-sized apatite of natural bone tissue.

ACKNOWLEDGMENT

Authors significantly acknowledge contribution of the University of Mines and Technology, Tarkwa and financial support of National Natural Science Foundation of China (No. 51671205).

REFERENCES

1. Alontseva, D., Azamatov, B., Safarova, Y., Voinarovych, S., & Nazenova, G. (2023). "A Brief Review of Current Trends in the Additive Manufacturing of Orthopedic Implants with Thermal Plasma-Sprayed Coatings to Improve the Implant Surface Biocompatibility", Coatings, 13(7), p. 1175.
2. Argyropoulou, E., Sakellariou, E., Galanis, A., Karampinas, P., Rozis, M., Koutas, K., Tsalimas, G., Vasiliadis, E., Vlamis, J., and Pneumaticos, S. (2024), "Porous Tantalum Acetabular Cups in Primary and Revision Total Hip Arthroplasty: What Has Been the Experience So Far? - A Systematic Literature Review", Biomedicines, 12(5), p. 959.
3. Balla, V. K., Banerjee, S., Bose, S. and Bandyopadhyay, A. (2010a), "Direct Laser Processing of a Tantalum Coating on Titanium for Bone Replacement Structures", Acta Biomaterialia, 6(6), pp. 2329–2334.
4. Balla, V. K., Bodhak, S., Bose, S. and Bandyopadhyay, A. (2010b), "Porous Tantalum Structures for Bone Implants: Fabrication, Mechanical and in Vitro Biological Properties". Acta Biomaterialia, 6(8), pp. 3349–3359.
5. Baltatu, M. S., Vizureanu, P., Sandu, A. V., Solcan, C., Hritcu, L. D. and Spataru, M. C. (2023) "Research Progress of Titanium-Based Alloys for Medical Devices", Biomedicines, 11(11), p. 2997.
6. Chen, P.-Y., McKittrick, J. and Meyers, M. A. (2012) "Biological Materials: Functional Adaptations and Bioinspired Designs. Progress in Materials Science, 57(8), pp. 1492–1704.
7. Chen, Q. and Thouas, G. A. (2015) "Metallic Implant Biomaterials". Materials Science and Engineering: R: Reports, 87, pp. 1–57.
8. Delloro, F., Jeandin, M., Jeulin, D., Proudhon, H., Faessel, M., Bianchi, L., Meillot, E. and Helfen, L. (2017) "A Morphological Approach to the Modelling of the Cold Spray Process", Journal of Thermal Spray Technology, 26(8), pp. 1838–1850.
9. Forero-Sandoval, I. Y., Franco-Bacca, A. P., Cervantes-Álvarez, F., Gómez-Heredia, C. L., Ramírez-Rincón, J. A., Ordonez-Miranda, J. and Alvarado-Gil, J. J. (2022), "Electrical and Thermal Percolation in Two-Phase Materials: A Perspective", Journal of Applied Physics, 131(23).
10. Gartner, F., Stoltenhoff, T., Schmidt, T. and Kreye, H. (2006) "The Cold Spray Process and Its Potential for Industrial Applications". Journal of Thermal Spray Technology, 15(2), pp. 223–232.
11. Gere, J. M. and Timoshenko, S. (2009) Mechanics of Materials (CL-Engineering), 402 p.
12. Xinting, K., Yaning, L., Guangzhong, L. and Ye, L., (2017), "Effect of Sintering Temperature on Properties of Tantalum Porous Materials", Rare Metal Materials and Engineering, 46(4), pp. 1092-1096.
13. Koivuluoto, H., Honkanen, M. and Vuoristo, P. (2010) "Cold-Sprayed Copper and Tantalum Coatings - Detailed FESEM and TEM Analysis". Surface and Coatings Technology, 204(15), pp. 2353–2361.
14. Kokubo, T. and Takadama, H. (2006) "How Useful is SBF in Predicting in Vivo Bone Bioactivity?" Biomaterials, 27(15), pp. 2907–2915.
15. Kumar, S., Vidyasagar, V., Jyothirmayi, A. and Joshi, S. V. (2016) "Effect of Heat Treatment on Mechanical Properties and Corrosion Performance of Cold-Sprayed Tantalum Coatings". Journal of Thermal Spray Technology, 25(4), pp. 745–756.
16. Lei, P., Qian, H., Zhang, T., Lei, T., Hu, Y., Chen, C. and Zhou, K. (2022), "Porous Tantalum Structure Integrated on Ti6Al4V Base by Laser Powder Bed Fusion for Enhanced Bony-Ingrowth Implants: In Vitro and In Vivo Validation", Bioactive Materials, 7, pp. 3-13.
17. Liu, A., Wang, C., Zhao, Z., Zhu, R., Deng, S., Zhang, S., Ghorbani, F., Ying, T., Yi, C., and Li, D. (2025), "Progress of Porous Tantalum Surface-Modified Biomaterial Coatings in Bone Tissue Engineering", Journal of Materials Science: Materials in Medicine, 36(1), pp. 1–14.

18. Loi, F., Córdova, L. A., Pajarinen, J., Lin, T. H., Yao, Z. and Goodman, S. B. (2016), "Inflammation, Fracture and Bone Repair". Bone, 86, pp. 119–130.
19. Melcher, F., Graupner, T., Gäbler, H. E., Sitnikova, M., Oberthür, T., Gerdes, A., Badanina, E. and Chudy, T. (2017), "Mineralogical and Chemical Evolution of Tantalum-(Niobium–Tin) Mineralisation in Pegmatites and Granites. Part 2: Worldwide Examples (Excluding Africa) and an Overview of Global Metallogenetic Patterns", Ore Geology Reviews, 89, pp. 946–987.
20. Meyers, M. A., McKittrick, J. and Chen, P. Y. (2013), "Structural Biological Materials: Citical Mechanics–Materials Connections". Science, 339(6121), pp. 773–779.
21. Moridi, A., Hassani-Gangaraj, S. M., Guagliano, M. and Dao, M. (2014), "Cold Spray Coating: Review of Material Systems and Future Perspectives". Surface Engineering, 30(6), pp. 369–395.
22. Neu, R., Maier, H., Böswirth, B., Elgeti, S., Greuner, H., Hunger, K., Kondas, J. and von Müller, A. (2023) "Investigations on Cold Spray Tungsten/Tantalum Coatings for Plasma Facing Applications", Nuclear Materials and Energy, 34, p. 101343.
23. Oryan, A., Alidadi, S., Moshiri, A. and Maffulli, N. (2014), "Bone Regenerative Medicine: Classic Options, Novel Strategies, and Future Directions". Journal of Orthopaedic Surgery and Research, 9(1), p. 18.
24. Papyrin, A., Kosarev, V., Klinkov, S., Alkhimov, A. and Fomin, V. M. (2006), Cold Spray Technology, 1st Edn, Elsevier, The Netherlands, pp. 27–28.
25. Schmidt, T., Gärtner, F., Assadi, H. and Kreye, H. (2006), "Development of a Generalized Parameter Window for Cold Spray Deposition". Acta Materialia, 54(3), pp. 729–742.
26. Shabalin, I. L. (2014), Ultra-High Temperature Materials. Springer, New York, NY, USA. pp. 237–531.
27. Wei, S., Bangchao, Y., Xuanhong, Z., Jianhua, M., Qifeng, P. and Xingwei, W. (2015), "Effect of Sintering Time on the Microstructure of Porous Tantalum". Rare Metal Materials and Engineering, 44(2), pp. 319–322.
28. Simchi, A., Tamjid, E., Pishbin, F. and Boccaccini, A. R. (2011), "Recent Progress in Inorganic and Composite Coatings with Bactericidal Capability for Orthopaedic Applications". Nanomedicine: Nanotechnology, Biology and Medicine, 7(1), pp. 22–39.
29. Takana, H., Li, H., Ogawa, K., Kuriyagawa, T. and Nishiyama, H. (2010), "Computational and Experimental Studies on Cavity Filling Process by Cold Gas Dynamic Spray", Journal of Fluids Engineering – Transactions of the ASME, 132(2), 021302.
30. Van Bael, S., Chai, Y. C., Truscello, S., Moesen, M., Kerckhofs, G., Van Oosterwyck, H., Kruth, J. P. and Schrooten, J. J. A. B. (2012), "The Effect of Pore Geometry on the In Vitro Biological Behaviour of Human Periosteum-Derived Cells Seeded on Selective Laser-Melted Ti6Al4V Bone Scaffolds", Acta Biomaterialia, 8(7), pp. 2824–2834.
31. Vilardell, A. M., Cinca, N., Concustell, A., Dosta, S., Cano, I. G. and Guilemany, J. M. (2015), "Cold Spray as an Emerging Technology for Biocompatible and Antibacterial Coatings: State of the Art", Journal of Materials Science, 50(13), pp. 4441–4462.
32. Nikolova, M. P. and Tzvetkov, I. (2025), "Influence of Deposition Temperature on Microstructure and Properties of Tantalum Oxide Sputtered Coatings. Materials", 18(9), p.1895.
33. Wang, X., Liu, W., Yu, X., Wang, B., Xu, Y., Yan, X. and Zhang, X. (2022), "Advances in Surface Modification of Tantalum and Porous Tantalum for Rapid Osseointegration: A Thematic Review", Frontiers in Bioengineering and Biotechnology, 10, p. 983695.
34. Xiong, Y., Zhuang, W., and Zhang, M. (2015), "Effect of Thickness of Cold Sprayed Aluminium Alloy Coating on the Adhesive Bond Strength with an Aluminium Alloy Substrate". Surface and Coatings Technology, 270, pp. 259–265.

ISSN No. 2454-6194 | DOI: 10.51584/IJRIAS |Volume X Issue XII December 2025

AUTHORS

Dr John Kojo Annan presently lectures at the Department of Electrical and Electronic Engineering of the University of Mines and Technology (UMaT), Tarkwa, Ghana. He holds PhD and MPhil degrees in Electrical and Electronic Engineering from UMaT. He also holds a BSc degree in Electrical and Electronic Engineering from the Kwame Nkrumah University of Science and Technology (KNUST), Kumasi. He is a member of the Institute of Electrical and Electronics Engineers, International Association of Engineers, and Society of Petroleum Engineers. His research interests are in Power Systems, Renewable Energy Systems, Computer Applications and Control, and Electrical Applications in Biomedical Systems.

Prof.Lawrence Gyansah lectures at Assemblies of God Institute of Higher Learning, Mechanical Engineering Dept., Kumasi, Ghana. He earned his PhD in Materials Science and Engineering from the University of Chinese Academy of Sciences (UCAS), China. He obtained his Master's degree in Mechanical Engineering at Montana Tech of the University of Montana, USA & University of Mines and Technology, Ghana. Prof. L. Gyansah obtained first-class honours BSc. in Mechanical Engineering at the Kwame Nkrumah University of Science and Technology, Kumasi, Ghana. His research areas include; super-alloy formations, mechanical behavior of metals and manufacturing of nano-composites. Proven track-record in research and development (R&D) in nanofabrications and coating technologies (such as thermal-barrier coatings, corrosion-resistant coatings, neutron shielding coatings, scratch-resistant coatings, and photocatalytic coatings).